J|A|C|S
ARTICLES

Published on Web 10/29/2009

A Single-Component Molecular Metal Based on a Thiazole Dithiolate Gold Complex

Nadine Tenn,[†] Nathalie Bellec,[†] Olivier Jeannin,[†] Lidia Piekara-Sady,[†,‡] Pascale Auban-Senzier,[§] Jorge Íñiguez,[||] Enric Canadell,[||] and Dominique Lorcy*[,†]

Sciences Chimiques de Rennes, UMR 6226 CNRS-Université de Rennes 1, Matière Condensée et Systèmes Electroactifs (MaCSE), Campus de Beaulieu, Bât 10A, 35042 Rennes cedex, France, Institute of Molecular Physics, Polish Academy of Sciences, Smoluchowskiego 17, 60-179 Poznan, Poland, Laboratoire de Physique des Solides, UMR 8502 CNRS-Université de Paris-Sud, Bat 510, F.91405 Orsay cedex, France, and Institut de Ciència de Materials de Barcelona (CSIC), Campus de la UAB, E-08193 Bellaterra, Spain

Received September 2, 2009; E-mail: dominique.lorcy@univ-rennes1.fr

Abstract: A single component molecular conductor has been isolated from electrocrystallization of the monoanionic gold bis(dithiolene) complex based on the *N*-ethyl-1,3-thiazoline-2-thione-4,5-dithiolate (Et-thiazdt) ligand. The crystal structure of the system exhibits layers built from parallel uniform one-dimensional stacks of the planar molecule. At room temperature and ambient pressure the system is semiconducting (0.33 $S \cdot cm^{-1}$) with a small activation energy. However, the single crystal conductivity is strongly pressure dependent reaching 1000 $S \cdot cm^{-1}$ at 21 kbar. At 13 kbar there is a crossover between semiconducting and metallic regimes. Thus, the present system is the first well characterized single-component molecular metal without TTF dithiolate ligands. First-principles DFT calculations show that the ground state is antiferromagnetic with a very small band gap. A simulation of the effect of pressure on the electronic structure provides a rationale for the observed variations of the conductivity and gives insight on how to further stabilize the metallic state of the system.

1. Introduction

Notwithstanding claims in the literature, the long date challenge of preparing a metallic solid based on neutral molecules without the help of any doping (a single-component molecular metal) was realized only recently.[1] An attractive feature of bis(dithiolene) metal complexes is their potential as precursors of these single-component molecular conductors.[1] Indeed, various neutral bis(dithiolene) complexes involving two TTF dithiolate ligands coordinated to a metal (M = Ni, Co, Cu, Pd, and Au) reported by Kobayashi and co-workers exhibit either semiconducting or metallic behavior.[1−3] On the other hand, only very few examples of neutral metal dithiolene complexes lacking this TTF backbone exhibit a similar single-component molecular conductor behavior. Apart from the molybdenum dithiolene cluster complexes reported by Llusar et al.,[4] all the others are square planar mononuclear gold bis(dithiolene) complexes with an odd number of total electrons, such as $[Au(bdt)_2]$,[5] $[Au(\alpha\text{-tpdt})_2]$,[6] and $[Au(F_2pdt)_2]$[7] (Chart 1). Such neutral gold complexes are not easily obtained from oxidation of the monoanionic species unless the dithiolene moieties are electron-rich ligands.

Chart 1

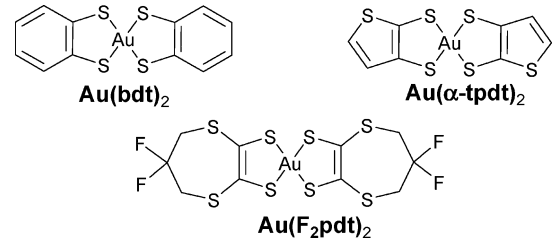

Recently, we have established an efficient approach to *N*-methyl-1,3-thiazoline-2-thione-4,5-dithiolate ligand (Me-thiazdt) and to its corresponding Ni and Pd bis(dithiolene) complexes $[M(Me\text{-}thiazdt)_2]^n$ (M = Ni, Pd and $n = -2, -1, 0$).[8] Their redox behavior indicates that Me-thiazdt is an electron-rich ligand and suggests that the neutral Au complexes are potentially isolable. As part of our ongoing interest on bis-(dithiolene) complexes involving the thiazdt backbone, we focused on the gold complexes, to evaluate their potential as a precursor of single-component molecular conductors. Being

[†] UMR 6226 CNRS-Université de Rennes 1.
[‡] Polish Academy of Sciences.
[§] UMR 8502 CNRS-Université de Paris-Sud.
[||] Institut de Ciència de Materials de Barcelona (CSIC).

(1) Kobayashi, A.; Fujiwara, E.; Kobayashi, H. *Chem. Rev.* **2004**, *104*, 5243–5264.
(2) Sasa, M.; Fujiwara, E.; Kobayashi, A.; Ishibashi, S.; Terakura, K.; Okano, Y.; Fujiwara, H.; Kobayashi, H. *J. Mater. Chem.* **2005**, *15*, 155–163.
(3) Okano, Y.; Zhou, B.; Tanaka, H.; Adachi, T.; Ohishi, Y.; Takata, M.; Aoyagi, S.; Nishibori, E.; Sakata, M.; Kobayashi, A.; Kobayashi, H. *J. Am. Chem. Soc.* **2009**, *131*, 7169–7174.
(4) (a) Llusar, R.; Uriel, S.; Vicent, C.; Clemente-Juan, J. M.; Coronado, E.; Gómez-Garcia, C. J.; Braïda, B.; Canadell, E. *J. Am. Chem. Soc.* **2004**, *126*, 12076–12083. (b) Llusar, R.; Triguero, S.; Polo, V.; Vicent, C.; Gómez-García, C. J.; Jeannin, O.; Fourmigué, M. *Inorg. Chem.* **2008**, *47*, 9400–9409.
(5) Schiødt, N. C.; Bjørnholm, T.; Bechgaard, K.; Neumeier, J. J.; Allgeier, C.; Jacobsen, C. S.; Thorup, N. *Phys. Rev. B* **1996**, *53*, 1773–1778.

Scheme 1

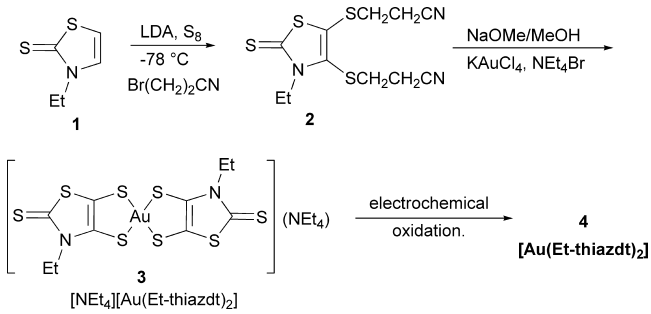

aware of solubility problems encountered with neutral gold complexes, we decided to investigate the synthesis of the *N*-ethyl rather than the *N*-methyl substituted ligand. Herein, we report the synthesis as well as the structural and electronic properties of the monoanionic and neutral radical species based on the [Au(Et-thiazdt)$_2$] complex, which exhibits metallic behavior under pressures higher that 13 kbar.

2. Results and Discussion

The synthesis of the monoanionic Au dithiolene complex **3**, [NEt$_4$][Au(Et-thiazdt)$_2$], was realized according to the synthetic pathway described in Scheme 1. First, the organic dithiolate hidden form **2** was prepared from *N*-ethyl-1,3-thiazoline-2-thione **1**[9] through the dilithiation of the thiazole core with LDA followed by the sequential addition of sulfur and 3-bromopropionitrile. Deprotection of the dithiolate was realized in the presence of sodium methanolate. Addition of KAuCl$_4$ followed by NEt$_4$Br allowed us to isolate, after recrystallization in acetonitrile, the Au dithiolene complex **3**, [NEt$_4$][Au(Et-thiazdt)$_2$], as a dark greenish crystalline solid amenable to single crystal X-ray diffraction.

As shown in Figure 1, the Au atom, located on an inversion center, is coordinated in a square planar environment, with a ligand bite angle of 91.83(5)° and with Au−S1 and Au−S2 bond distances of 2.3321(16) and 2.3287(15) Å, respectively, comparable to those observed for other monoanionic homoleptic gold dithiolene complexes. The thiazole cores are planar, apart from the ethyl groups which point out of the plane.

Interestingly, the metallacycles are nonplanar and are folded along the S···S axis with an angle of ∼10°. Moreover, only the *trans* isomer is observed in the solid state even if the *cis* and *trans* isomers are susceptible to exist due to the dissymmetry of the dithiolene ligands as observed for other Ni and Pd homoleptic complexes based on Me-thiazdt.[8]

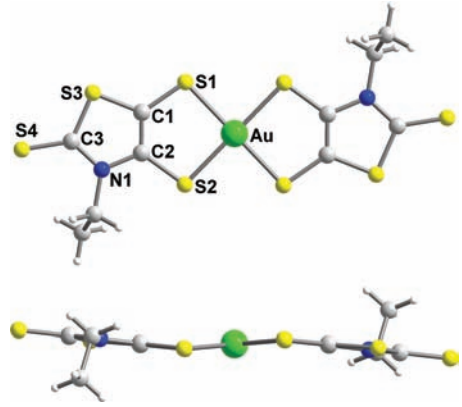

Figure 1. Molecular structure of the anion [Au(Et-thiazdt)$_2$]$^-$ in crystals of **3**.

Table 1. Comparison of the Bond Lengths in Monoanionic and Neutral [Au(Et-thiazdt)$_2$]

	[Au(Et-thiazdt)$_2$] in **3**	[Au(Et-thiazdt)$_2$] in **4**
Au−S1	2.3321(16)	2.3196(13)
Au−S2	2.3287(15)	2.3186(14)
S1−C1	1.744(6)	1.713(5)
S2−C2	1.760(5)	1.720(6)
C1−C2	1.332(8)	1.372(8)
C2−N1	1.416(7)	1.390(7)
C1−S3	1.731(6)	1.738(5)
N1−C3	1.356(7)	1.370(7)
S3−C3	1.743(6)	1.749(6)
C3−S4	1.658(6)	1.641(6)

Cyclic voltammogram of **3** has been recorded in CH_2Cl_2. Upon anodic investigation, two close reversible oxidation waves are observed at $E^1 = 0.52$ V and $E^2 = 0.65$ V vs SCE. The two processes correspond respectively to the oxidation of the monoanion into the neutral radical and to the oxidation of the neutral radical into the monocation species. Upon cathodic scan, an irreversible reduction wave is observed at $E = -0.90$ V corresponding to the reduction of the monoanion into the dianion. It is worth noting that investigation of the redox behavior of **3** in CH_3CN instead of CH_2Cl_2 shows only one reversible oxidation wave at 0.44 V and one reversible reduction wave at −0.73 V vs SCE. The influence of the ligand Et-thiazdt on the overall electron donating ability of the complex **3** stands comparison with the ligands α-tpdt[6] and F$_2$pdt.[7]

Oxidation of **3** has been realized either chemically using ferricinium hexafluorophosphate or iodine as oxidizing agent or electrochemically. The chemical approach leads to insoluble powders while electrocrystallization affords crystals growing at the anode upon application of a current intensity of 0.5 μA in the presence of NBu$_4$PF$_6$ as a supporting electrolyte. The neutral complex [Au(Et-thiazdt)$_2$], **4**, crystallizes in the monoclinic system, space group $P2_1/a$. X-ray structure analysis shows that the complex is in a neutral radical state and planar. Moreover, as for the monoanionic species, the *trans* isomer is obtained.

As both structures were obtained with high precision, it is now possible to compare the molecular structures of the complex on the monoanionic and neutral states and to analyze the evolution of the geometrical characteristics of the [Au(Et-thiazdt)$_2$] core upon oxidation (Table 1). Modifications of the bond lengths occur essentially on the metallacycle rings. For instance, the Au−S and S−C bonds are shortened while the C=C bond is lengthened. Apart from this C=C bond, the other bonds in the thiazole ring are not significantly modified. This tends to indicate the localization of the spin density on the dithiolene moieties, as observed with the few examples of gold dithiolene complexes reported so far where both monoanionic and neutral forms were characterized, that is [Au(α-tpdt)$_2$],[6] [Au(dddt)$_2$],[10,11] [Au(F$_2$pdt)$_2$],[7] and [AuL$_2$] with L = 1,2-di-(4-*tert*-butylphenyl)ethylene-1,2-dithiolate.[12] On the other hand, no significant modifications of the bond angles are observed between both species as, for example, the ligand bite angle remains constant at 91.83(5)° in **3** and 91.88(5)° in **4**. In the solid state, the neutral radical complexes form uniform stacks (at 100 K) along *b* with a mean plane-to-plane distance of 3.57 Å (Figure 2).

Within the stacks, a lateral slip is observed between neighboring complexes with the shortest intermolecular S···S contact

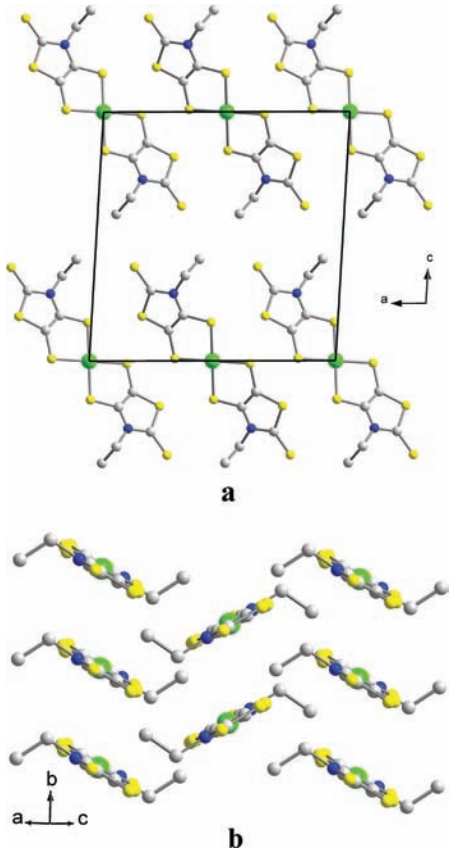

Figure 2. Projection view along *b* of the unit cell of [Au(Et-thiazdt)$_2$] **4** (a); detail of the stacking along *b* (b).

at 3.841(6) Å (Figure 3a). Several S···S contacts notably shorter than the sum of van der Waals radii (3.70 Å) are observed between the stacks as represented in Figure 3b. Among the other neutral gold complexes two types of overlap mode have been observed when the complexes arrange in uniform chains, either a longitudinal slip for [Au(F$_2$pdt)$_2$][7] or a lateral slip for [Au(bdt)$_2$].[13,5] Interestingly, compared with **4**, the latter exhibits a smaller number of short S···S contacts between the stacks.

Electrical resistivity was measured on single crystals of **4** along the *b* direction (axis of the needle). At room temperature and ambient pressure, the conductivity is estimated to σ_{RT} (1 bar) = 0.33 S·cm^{-1}. It is actually the highest conductivity measured on single crystals for this type of neutral gold dithiolene complexes without a TTF backbone. However,

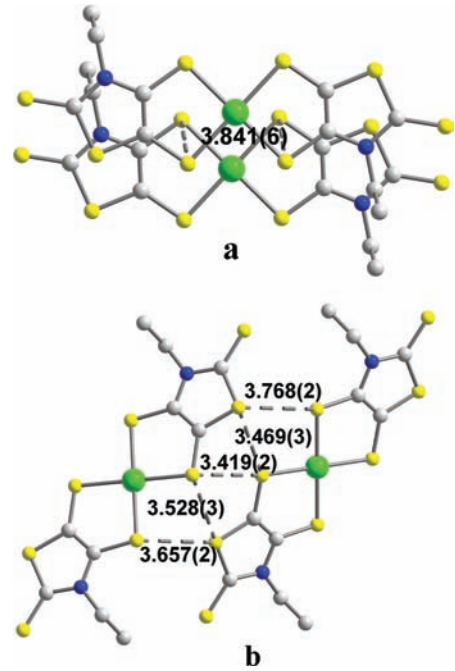

Figure 3. View of the short S···S contacts between neighboring [Au(Et-thiazdt)$_2$] (a) within the stacks and (b) between two neighboring stacks.

upon cooling, a semiconducting behavior is observed with a small activation energy of 0.12 eV (Figure 4a). The conductivity of **4** at room temperature was found to be strongly pressure dependent, reaching 1000 S·cm^{-1} at 21 kbar (see insert of Figure 4a). An exponential pressure dependence is first observed up to 13 kbar, and then the conductivity increases linearly with pressure. These two distinct behaviors correspond to the crossover between a semiconducting temperature dependence below 13 kbar and a conducting behavior for higher pressures, when cooling down from room temperature (see Figure 4b). As already observed in (TMTTF)$_2$X charge transfer salts,[14] electronic correlations are responsible for the one-dimensional (1D) Mott localization which is dominant for the lowest pressures and is depressed when the increase in interchain coupling allows 2D conduction. At lower temperature, a sharp metal to insulator transition is observed at 13 and 14 kbar below 70 and 40 K, respectively, and is rapidly suppressed with pressure. These features could be related to a Peierls transition triggered by the nesting of the Fermi surface (see discussion below), as recently reported for (EDT-TTFCONMe$_2$)$_2$X salts.[15] At higher pressures, only a slight localization is detected below 20 K for 15 kbar and below 7 K for 17 kbar. No sign of superconductivity could be detected down to 60 mK for this last pressure. To explain the absence of superconductivity in this material, one can notice that the lowest resistivity value reached at 4.5 K and 21 kbar is 0.079 mΩ·cm, with a resistivity ratio of only 10 between 290 and 4.5 K, while the residual resistivity measured along the stacking axis at T_c for superconducting (TMTSF)$_2$X salts is around 0.005 mΩ·cm without any saturation.

The magnetic susceptibility of **4** was measured with a SQUID magnetometer in the temperature range 2−300 K. The para-

(6) Belo, D.; Alves, H.; Lopes, E. B.; Duarte, M. T.; Gama, V.; Henriques, R. T.; Almeida, M.; Pérez-Benítez, A.; Rovira, C.; Veciana, J. *Chem.—Eur. J.* **2001**, *7*, 511–519.
(7) Dautel, O. J.; Fourmigué, M.; Canadell, E.; Auban-Senzier, P. *Adv. Funct. Mater.* **2002**, *12*, 693–698.
(8) Eid, S.; Fourmigué, M.; Roisnel, T.; Lorcy, D. *Inorg. Chem.* **2007**, *46*, 10647–10654.
(9) Roussel, C.; Gallo, R.; Chanon, M.; Metzger, J. *Bull. Soc. Chim. Fr.* **1971**, *5*, 1902–1907.
(10) Schultz, A. J.; Wang, H. H.; Soderholm, L. C.; Sifter, T. L.; Williams, J. M.; Bechgaard, K.; Whangbo, M.-H. *Inorg. Chem.* **1987**, *26*, 3757–3761.
(11) Geiser, U.; Schultz, A. J.; Wang, H. H.; Beno, M. A.; Williams, J. M. *Acta. Crystallogr., Sect. C* **1988**, *44*, 259–262.
(12) Kokatam, S.; Ray, K.; Pap, J.; Bill, E.; Geiger, W. E.; Le Suer, R. J.; Rieger, P. H.; Weyhermüller, T.; Neese, F.; Wieghardt, K. *Inorg. Chem.* **2007**, *46*, 1100–1111.
(13) Rindorf, G.; Thorup, N.; Bjørnholm, T.; Bechgaard, K. *Acta Crystallogr., Sect. C* **1990**, *46*, 1437–1439.
(14) Moser, J.; Gabay, M.; Auban-Senzier, P.; Jérome, D.; Bechgaard, K.; Fabre, J. M. *Eur. Phys. J. B* **1998**, *1*, 39–46.
(15) Auban-Senzier, P.; Pasquier, C. R.; Jérome, D.; Suh, S.; Brown, S. E.; Mézière, C.; Batail, P. *Phys. Rev. Lett.* **2009**, *102*, 257001.

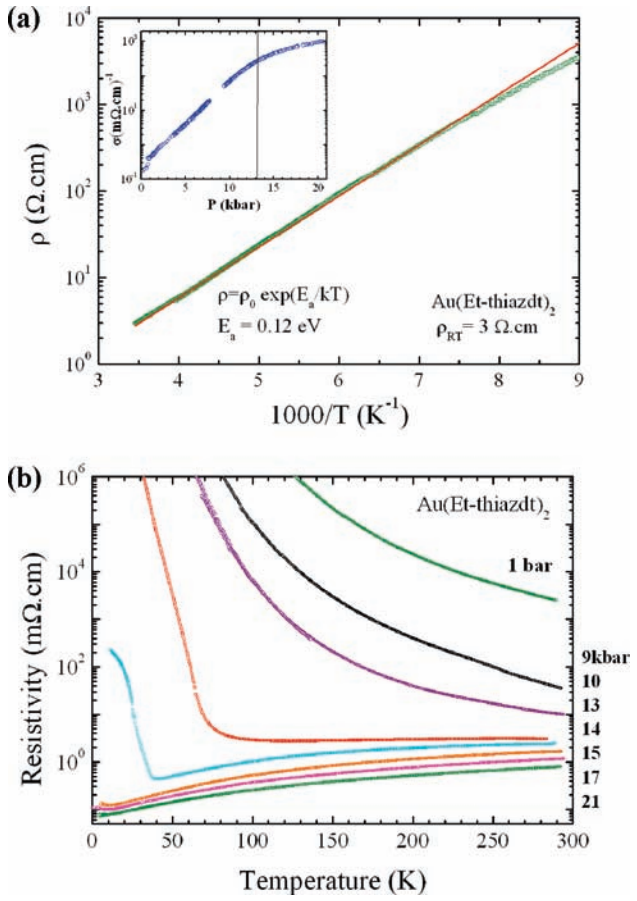

Figure 4. (a) Resistivity data of [Au(Et-thiazdt)$_2$] along the *b* axis at ambient pressure plotted as ρ versus the inverse temperature; the line is a linear fit of the data giving an activation energy of 0.12 eV. Insert: Pressure dependence of the conductivity of [Au(Et-thiazdt)$_2$] at room temperature. (b) Temperature dependence of the resistivity of [Au(Et-thiazdt)$_2$] at different applied pressures.

magnetic susceptibility corrected for the Pascal diamagnetic term (1.10×10^{-4} cm^3 mol^{-1} at room temperature) is temperature independent, in accordance with a Pauli-type susceptibility of a good conductor in agreement with spin-charge separation in 1D correlated systems.[16] A Curie tail at the lower temperatures corresponds to only 0.6% of $S = {}^1/_2$ species attributable to paramagnetic defaults.

The CW X band EPR spectrum of the polycrystalline gold neutral complex displays at room temperature a single broad signal centered at $g \approx 2$ and a line width of 930 G (Figure 5). The EPR spectrum at low temperature (77 K) shows noticeable line narrowing down to 190 G, as compared to the room temperature spectrum. This ~5 times smaller line width at low temperatures is associated with the conducting properties of the sample. Indeed a similar behavior, broad EPR line narrowing with decreasing temperature, was already observed with highly conducting gold dithiolene complexes such as [Au(tmdt)$_2$][17] and [Au(dtdt)$_2$][18] with a TTF backbone or [Au(α-tpdt)$_2$][17] without the TTF core.[19]

First-principles band structure calculations were carried out to understand how the crystal structure and physical properties of **4** are correlated. The first question to answer is that of the ground state of the material. Using the experimental crystal structure we were able to find both metallic and antiferromagnetic (AFM) states which differ by a tiny energy difference of 5 meV per unit cell. The localized AFM state is the ground state and is made of stacks with molecules with an unpaired spin up and down alternating along *b*. The calculated band structure for this nonmetallic state is reported in Figure 6 (every band in this figure is really the superposition of two bands, one associated with spin up and the other with spin down). As noted for other gold bis(dithiolene) complexes, the single occupied molecular orbital (SOMO) and the orbital immediately below (SOMO-1) differ by an energy which is of the same order of magnitude as the intermolecular transfer integrals. This leads to the overlap of the SOMO and SOMO-1 bands with the consequence that, in contrast with most molecular conductors, two bands per molecule must be explicitly considered. Although the crystallographic unit cell contains only two molecules, we had to double this unit cell to be able to describe the antiferromagnetic state. Consequently, the band structure of Figure 6 contains eight bands, four originating from the SOMO and four from the SOMO-1. Since every molecule contributes with three electrons to the bands of Figure 6, six pairs of bands should be filled. Note the small indirect gap separating the sixth and seventh pairs of bands. Although *strictu sensu* there is an indirect band gap (between Γ and the vicinity of M) and the conduction

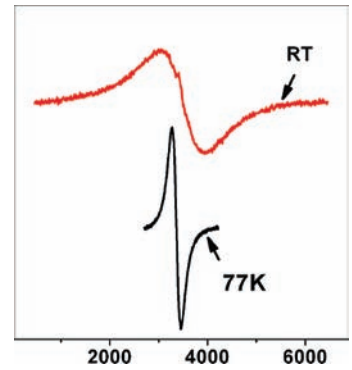

Figure 5. X-band EPR spectra of a polycrystalline sample of [Au(Et-thiazdt)$_2$] **4** (a) at room temperature and (b) 77 K.

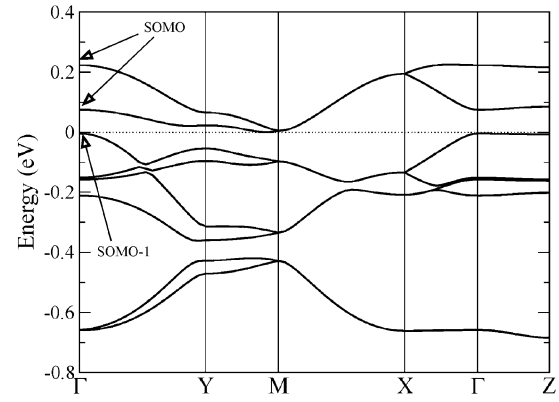

Figure 6. Band structure for the antiferromagnetic ground state of **4**. The dotted line refers to the highest occupied level of the system. Γ, X, Y, Z, and M refer to the (0, 0, 0), ($^1/_2$, 0, 0), (0, $^1/_2$, 0), (0, 0, $^1/_2$), and ($^1/_2$, $^1/_2$, 0) points of the monoclinic Brillouin zone.

(16) Jérome, D. *Chem. Rev.* **2004**, *104*, 5565–5591.
(17) Suzuki, W.; Fujiwara, E.; Kobayashi, A.; Fujishiro, Y.; Nishibori, E.; Takata, M.; Sakata, M.; Fujiwara, H.; Kobayashi, H. *J. Am. Chem. Soc.* **2003**, *125*, 1486–1487.
(18) Nunes, J. P. M.; Figueira, M. J.; Belo, D.; Santos, I. C.; Ribeiro, B.; Lopes, E. B.; Henriques, R. T.; Vidal-Gancedo, J.; Veciana, J.; Rovira, C.; Almeida, M. *Chem.—Eur. J.* **2007**, *13*, 9841–9849.
(19) Coulon, C.; Clérac, R. *Chem. Rev.* **2004**, *104*, 5655–5687.

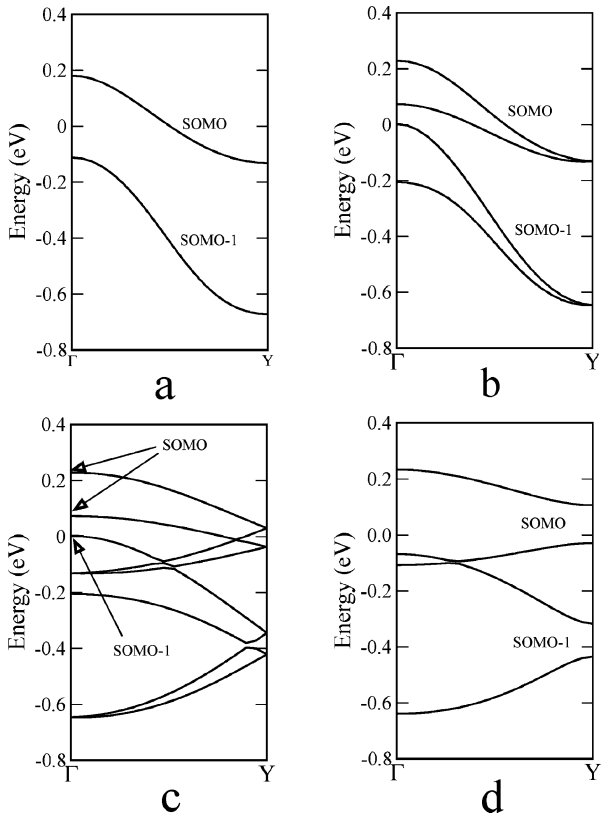

Figure 7. Band structure for (a) metallic single chain of molecules (one molecule per repeat unit); (b) metallic double chain of molecules (two molecules per repeat unit); (c) metallic double chain with a double unit cell (four molecules per repeat unit); (d) antiferromagnetic single chain (two molecules per repeat unit).

should be activated, the material may be considered as a semimetal, thus explaining the fact that whereas the conductivity is activated (although with a small activation energy), the magnetic susceptibility shows a Pauli-type paramagnetic behavior, typical of metallic systems. It is interesting to note that Terakura and co-workers[20] have also found an AFM ground state separated by a very small energy difference from the metallic state for $Au(tmdt)_2$, one of the very few gold-based single-component molecular metals (although in that case incorporating TTF dithiolate ligands). In agreement with previous work[7,10] noting the very weak participation of the gold orbitals into the SOMO, we find that only 3.4% of the total magnetic moment is associated with gold. In contrast up to 10.7% of the total moment corresponds to individual sulfur atoms (S1, S2, and S4) and up to 8.3% to individual carbon atoms (C1 and C2).

To understand the transport properties as a function of pressure and try to stabilize the metallic state of similar single-component conductors, it is important to understand the origin of the bands near the highest occupied level in Figure 6. Since the energy dispersion along the stacks direction (b^*) is considerably larger than those along the interstack and interlayer directions (a^* and c^*, respectively), we will just consider the band structure along the stacks direction. Shown in Figure 7a is the band structure for a single chain with the SOMO band above the SOMO-1 one. The band structure of a double chain is shown in Figure 7b. Every band in Figure 7a becomes a pair of bands which touch at the Y point. If there was no interaction between the two chains, the band structure would be two pairs of identical bands. Since the interchain interaction along a^* is not nil, the two bands of each pair separate, the interaction being maximum at Γ. When a double chain with two molecules per chain is used, the calculated band structure is that of Figure 7c. Of course the band structures of Figure 7b and 7c must be identical. The use of a double unit cell simply induces a folding of the bands[21] in such a way that the Γ and Y points of Figure 7b are now found at the Γ point of the new (smaller) Brillouin zone. Consequently, the eight bands in Figure 7c can easily be traced back to the SOMO and SOMO-1 of an isolated chain: the upper first, second, fourth, and fifth bands at Γ originate from the SOMO band of the isolated chain, whereas the other originate from the SOMO-1 band of the isolated chain. How does the appearance of an antiferromagnetic ordering along the chains modify this description? This can be easily understood by comparing the band structures of Figures 7a and 7d which are those for metallic and AFM single chains. The band structure of Figure 7d is simply obtained from that of Figure 7a by first folding (two molecules in the repeat unit for the AFM chain) and then opening a gap at the Y point. The process is very similar to the opening of a gap through a Peierls distortion. However, whereas in the Peierls distortion the perturbation responsible for the gap opening is electron−phonon coupling and, consequently, there is a structural change (a dimerization), for the AFM chain the perturbation is electron−electron repulsion and there is no structural change. Another difference is that the up and down bands for the metallic state are delocalized over the two molecules of the unit cell, whereas for the AFM state the up and down bands are localized on different molecules of the unit cell. We are now ready to come back to the band structure of the AFM ground state of **4** (Figure 6). Looking at the eight bands along the Γ → Y direction, it is clear that these bands are simply those of Figure 7c after opening gaps at the Y point as a result of the AFM ordering. An important point for the further discussion is that the two upper bands at Γ in Figure 6 originate from the SOMO whereas the third originates from the SOMO-1.

To understand the experimental fact that the system becomes a metal under moderate pressures, we have run simulations for slightly compressed cells along the *a*- and *b*-directions. In these simulations the molecules were moved rigidly along the chosen directions. The calculated band structures for the AFM state when the molecules get closer by 0.2 Å are shown in Figure 8. The nature of the ground state is especially sensitive to compression along the *b*-direction. Compression favors two effects: (i) the closing of the indirect gap of the AFM state and (ii) the energetic preference of the metallic solution with perfectly paired spins. The band structure for the metallic state is practically identical to those of Figure 8 except for the fact that the bands are doubly degenerate along the Y → M direction. Our calculations thus suggest that metallization under pressure occurs via the closing of the indirect gap. That is, an AFM semimetallic state appears under pressure, but under low additional pressure the system evolves into a diamagnetic metal. In the metallic state the upper part of the third band from the top becomes filled. As discussed above, this band originates from the SOMO-1, whereas the two upper bands at Y originate from the SOMO. Thus, when the metallization occurs, the

(20) Ishibashi, S.; Terakura, K.; Kobayashi, A. *J. Phys. Soc. Jpn.* **2008**, *77*, 24702.

(21) Rousseau, R.; Gener, M.; Canadell, E. *Adv. Funct. Mat.* **2004**, *14*, 201–214.

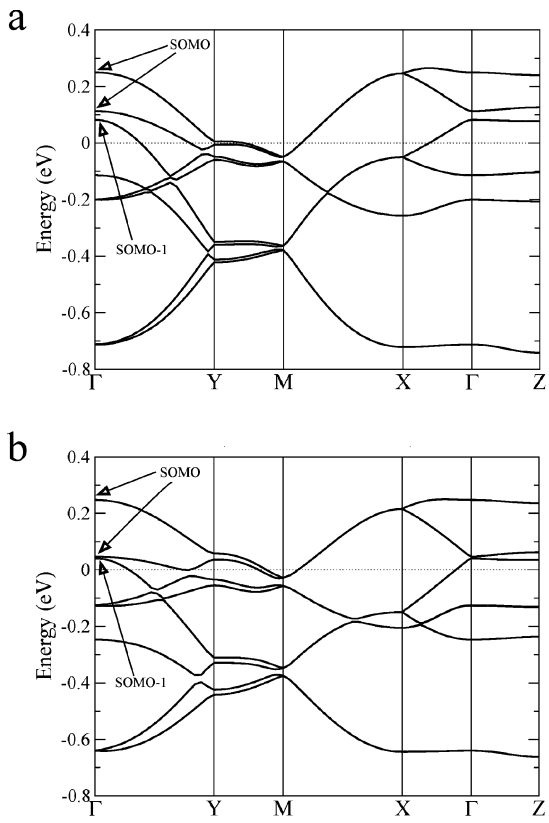

Figure 8. Simulation of the pressure effect: band structure calculated for the antiferromagnetic state of **4** when the molecules are rigidly brought closer by 0.2 Å along (a) the stacks direction and (b) the *a* interstacks direction. The dotted lines refer to the Fermi level.

internal electron transfer which characterizes the two-band single-molecule metals[22] comes about.

At the initial stages of the transfer, where the filling of the SOMO-1 band is still very small, the unfolded band structure of the metallic state is that of a pseudo-one-dimensional system along *b*. Consequently, the Fermi surface contains two pairs of warped lines perpendicular to *b* (with very small closed hole pockets arising from the emptying of the top of the SOMO band) and has a strong driving force for a charge (or spin) density wave modulation which will destroy again the metallic state.[23] This metal to insulator transition should lead to a sharp upturn in the resistivity curve, exactly as it occurs in Figure 4b for pressures of 13−14 kbar. At the initial stages of the metallization, the size of the closed pockets will be very small and most certainly commensuration effects will dominate leading to a doubling of the periodicity along the *b*-direction. When the pressure increases and the overlap of the SOMO and SOMO-1 bands increases, as shown for instance in Figure 8, the transfer from the SOMO-1 to the SOMO bands increases, the area of the closed hole pockets is larger, and, consequently, since the filling of the SOMO pseudo-one-dimensional bands increasingly differs from one-half, the modulation which could stabilize the system by destroying the pseudo-one-dimensional bands becomes incommensurate with the lattice. The driving force for such incommensurate modulations is smaller than that for the commensurate ones and even more under pressure. In addition, the closed pockets, which are now larger, would remain since they have not been affected by the modulation. Consequently, at pressures slightly higher than those under which the metal to insulator transition occurs, the metallic state will be definitely stabilized.

The previous discussion not only provides a rationalization of the transport properties under pressure but also suggests how the metallic state may be stabilized under ambient pressure. As discussed above the key feature is the rise in energy of the third band (SOMO) around the Γ point. There are two ways to induce such a rise in energy. The first is by increasing the strength of the interactions along the stacks. This can occur by chemical means by substituting selenium for sulfur atoms in the central core of the molecule. Second, as noted in our discussion of Figure 7b, the splitting of the two bands at Γ is due to the interstack interactions along the transverse direction (*a*). Thus, increasing these interactions by using a less bulkier methyl substituent could be another way to stabilize the metallic state. However our model simulations suggest that the first alternative would likely be more efficient.

3. Conclusion

In conclusion, we have reported here the synthesis of an original neutral gold dithiolene complex with a thiazole backbone, [Au(Et-thiazdt)$_2$], and showed through physical characterizations and first-principles band structure calculations that, in the solid state, it behaves as a single-component molecular conductor with a rich (pressure, temperature) phase diagram. This result indicates that the thiazole dithiolate ligand is a useful building block for the elaboration of neutral gold complexes exhibiting promising properties. In light of the numerous structural modifications which can be brought to the thiazole core, either through the nitrogen substituent or on the chelating part (for instance, diselenolate instead of dithiolate), as well as the fact that antiferromagnetic, metallic, and charge or spin density wave states are in strong competition for **4**, this work widens perspectives from both chemical and physical points of view. Extensions following these lines will be reported in due course.

4. Experimental Section

4.1. General. All reagents were used as purchased. The thiazoline-2-thione **1** was synthesized according to a literature procedure.[9] All air-sensitive reactions were carried out under an argon atmosphere. Melting points were measured on a Kofler hot-stage apparatus and are uncorrected. ^{1}H NMR and ^{13}C NMR spectra were recorded on a Bruker AV300III spectrometer. Chemical shifts are quoted in parts per million (ppm) referenced to tetramethylsilane. Mass spectra were recorded with a Varian MAT 311 instrument by the Centre Régional de Mesures Physiques de l'Ouest, Rennes. Elemental analyses were performed at the Centre Régional de Mesures Physiques de l'Ouest, Rennes. Tetrahydrofuran was distilled from sodium-benzophenone. Column chromatography was performed using silica gel Merck 60 (70−260 mesh). Cyclic voltammetry was carried out on a 10^{-3} M solution of the complex in CH_3CN or in CH_2Cl_2, containing 0.1 M nBu$_4$NPF$_6$ as a supporting electrolyte. Voltammograms were recorded at 0.1 V s^{-1} on a platinum disk electrode ($A = 1$ mm^2). The potentials were measured versus Saturated Calomel Electrode.

4.1.1. Preparation of 3,3′-[(3-Ethyl-2-thioxo-2,3-dihydro-1,3-thiazole-4,5-diyl)bis(thio)]dipropanenitrile 2. To a −10 °C cooled solution of thiazoline-2-thione **1** (3.45 mmol, 0.5 g) in dry THF (40 mL) was added a solution of LDA freshly prepared from *n*-BuLi (5.2 mmol, 3.25 mL, 1.6 M in hexane) and diisopropylamine (5.2 mmol, 0.74 mL) in 15 mL of dry THF. After stirring for 30 min at

(22) (a) Canadell, E.; Rachidi, I. E.-I.; Ravy, S.; Pouget, J.-P.; Brossard, L.; Legros, J.-P. *J. Phys. (France)* **1989**, *50*, 2967–2981. (b) Canadell, E. *New. J. Chem.* **1997**, *21*, 1147–1159. (c) Rovira, C.; Novoa, J. J.; Mozos, J.-L.; Ordejón, P.; Canadell, E. *Phys. Rev. B* **2002**, *65*, 81104.
(23) (a) Jérome, D.; Schulz, H. J. *Adv. Phys.* **1982**, *31*, 299. (b) Canadell, E.; Whangbo, M.-H. *Chem. Rev.* **1991**, *91*, 965–1034.

−10 °C, S_8 (5.2 mmol, 0.17 g) was added and the solution was stirred for an additional 30 min. To the medium a solution of LDA (6.9 mmol, 4.3 mL of *n*-BuLi in hexane added to 6.9 mmol, 1.0 mL of diisopropylamine in 15 mL of dry THF) was added. The reaction mixture was stirred at −10 °C for 3 h, and sulfur S_8 (6.9 mmol, 0.22 g) was added. After 30 min, 3-bromopropionitrile (0.86 mL, 10.3 mmol) was added and the reaction mixture was stirred overnight. The solvent was evaporated *in vacuo*, and the residue was extracted with CH_2Cl_2. The concentrated solution was purified by chromatography on silica gel using CH_2Cl_2 as eluant to afford **2** as a light brown precipitate in 40% yield. Mp 112−114 °C. ^{1}H NMR (300 MHz, $CDCl_3$) δ 1.40 (t, 3H, CH_3, $^3J = 7$ Hz), 2.78 (t, 4H, CH_2CN, $^3J = 7$ Hz), 3.15 (t, 2H, SCH_2, $^3J = 7$ Hz), 3.21 (t, 2H, SCH_2, $^3J = 7$ Hz), 4.51 (q, 2H, CH_2, $^3J = 7$ Hz); ^{13}C RMN (75 MHz, $CDCl_3$) δ = 13.2 (CH_3CH_2), 18.6 (CH_2CN), 18.7 (CH_2CN), 31.7 (SCH_2), 32.4 (SCH_2), 44.9 (NCH_2), 117.20 (CN), 117.24 (CN), 125.6 (=C), 135.6 (=C), 187.3 (C=S); HRMS Calcd for $C_{11}H_{13}N_3S_4$ [$M^{+\bullet}$] 314.9992, found 314.9993. Anal. Calcd for $C_{11}H_{13}N_3S_4$: C,41.88; H, 4.15; N, 13.32; S, 40.65. Found: C, 41.90; H, 4.13; N, 13.10; S, 40.81.

4.1.2. Preparation of [NEt_4][Au(Et-thiazdt)$_2$] 3. To a dry two-necked flask containing thiazoline-2-thione **2** (0.25 g, 0.79 mmol), 7 mL of 1 M NaOMe in MeOH were added under nitrogen at room temperature. The mixture was stirred for 30 min, and a solution of $KAuCl_4$ (0.16 g, 0.43 mmol) in 5 mL of MeOH was added to the medium. The reaction mixture was stirred for 2 h at room temperature, and a solution of NEt_4Br (0.10 g, 0.5 mmol) was added. After an additional stirring overnight, the precipitate was filtered, washed with MeOH, and recrystallized in CH_3CN to afford **3** in 27% yield as dark crystals. Mp = 210 °C; ^{1}H NMR (CD_3CN, 200 MHz) δ 1.21 (m, 12H, CH_3), 1.25 (t, 6H, CH_3, $^3J = 7.1$ Hz), 3.16 (q, 8H, CH_2, $^3J = 7.3$ Hz), 4.13 (q, 4H, CH_2, $^3J = 7.1$ Hz); HRMS Calcd for $C_{26}H_{50}N_4S_8Au$ [$2C^+$, A^-]$^+$ 871.1467, found 871.1467. Anal. Calcd for $C_{18}H_{30}N_3S_8Ni$: C, 29.14; H, 4.08; N, 5.66; S, 34.57. Found: C, 28.76; H, 4.05; N, 5.58; S, 34.46.

4.2. Electrocrystallization. Crystals of [Au(Et-thiazdt)$_2$] **4** were prepared electrochemically under an argon atmosphere using a standard H-shaped cell with Pt electrodes. An acetonitrile solution of [NEt_4][Au(Et-thiazdt)$_2$] **3** (20 mg) was placed in the anodic compartment, and nBu_4NPF_6 in both compartments. Black needle crystals of **4**, suitable for X-ray diffraction studies, were obtained on the anode upon application of a constant current of 0.5 μA for 10 days.

4.3. Crystallography. Crystals of **3** were mounted on the top of a thin glass fiber with Araldite glue, and crystals of **4** were picked up with a cryoloop and then frozen at 100 K under a stream of dry N_2. Data were collected on an APEX II Bruker AXS diffractometer with graphite-monochromated Mo Kα radiation ($\lambda = 0.710\,73$ Å). Structures were solved by direct methods (SIR97)[24] and refined (SHELXL-97)[25] by full-matrix least-squares methods, as implemented in the WinGX software package.[26] Absorption corrections were applied. Hydrogen atoms were introduced at calculated positions (riding model, included in structure factor calculations but not refined). Details of the final refinements are given in Table 2 for all compounds.

4.4. Conductivity Measurements. Electrical resistivity was measured on single crystals in a four point configuration with annular contacts made by gold evaporation and gold wires attached with silver paste. Both ac (low-frequency lock-in detection) and dc measurements were performed with current intensities varying from 1 to 0.01 μA, depending on the resistance of the sample. Hydrostatic pressures up to 21 kbar were applied at room temperature in a NiCrAl clamp cell using Daphne 7373 silicone oil as the pressure transmitting medium. The pressure was determined, at room temperature, using a manganin resistance gauge located in the pressure cell close to the sample. The pressures indicated here are room temperature values, and the loss of pressure occurring during cooling is estimated to be 2 kbar. The sample in the pressure cell or at ambient pressure was then slowly cooled down to 4 K. Only one experiment at 17 kbar was performed in a dilution refrigerator down to 60 mK.

Table 2. Crystallographic Data[a]

compound	3	4
formula	$C_{18}H_{30}AuN_3S_8$	$C_{10}H_{10}AuN_3S_8$
FW ($g\cdot mol^{-1}$)	1483.96	611.65
crystal system	monoclinic	monoclinic
space group	$P2_1/c$	$P2_1/a$
a (Å)	9.5917(4)	14.060(5)
b (Å)	13.0319(5)	4.0593(6)
c (Å)	10.8481(4)	14.259(2)
α (deg)	90	90
β (deg)	96.686(3)	93.524(5)
γ (deg)	90	90
V (Å^3)	1346.77(9)	812.3(2)
T (K)	293(2)	100(2)
Z	1	2
D_{calc} ($g\cdot cm^{-3}$)	1.829	2.501
μ (mm^{-1})	6.095	10.075
total refls.	17219	6119
abs. corr.	multiscan	multiscan
unique refls. (R_{int})	3075 (0.0692)	1823 (0.0433)
unique refls.	2131 ($I > 2\sigma(I)$)	1546 ($I > 2\sigma(I)$)
R_1, wR_2	0.0383, 0.0720	0.0322, 0.0664
R_1, wR_2 (all data)	0.0714, 0.0813	0.0421, 0.0702
GoF	1.072	1.061

[a] $R_1 = \Sigma||F_o| - |F_c||/\Sigma|F_o|$; $wR_2 = [\Sigma w(F_o^2 - F_c^2)^2/\Sigma wF_o^4]^{1/2}$.

4.5. Computational Details. We have used the spin-polarized Generalized Gradient Approximation[27] (σ-GGA) approach to Density Functional Theory[28] (DFT) as implemented in the *Vienna Ab Initio Simulation Package* (VASP).[29] We used the Projector Augmented Wave[30] method to represent the ionic cores, solving explicitly for the following electrons: 5*d* and 6*s* of Au, 3*s* and 3*p* of S, 2*s* and 2*p* of N and C, and 1*s* of H. Electronic wave functions were represented with a plane wave basis truncated at 400 eV. A careful convergence test for Brillouin Zone integrations was necessary. Accurate energy differences between various (e.g., antiferromagnetic vs metallic) electronic solutions were obtained using Γ-centered 4 × 8 × 4 *k*-point grids for the simulation cell with four molecules in it, which results from the crystalline cell (two molecules) and an antiferromagnetic ordering along *b*.

Acknowledgment. L.P.-S. thanks the CNRS for financial support for her Associated Researcher position in Rennes. We acknowledge Claude Pasquier for his cooperation in the interpretation of the resistivity data. This work was supported by DGES-Spain (Project FIS2006-12117-C04-01). We made use of the computational facilities provided by CESCA and CESGA.

Supporting Information Available: X-ray crystallographic files in CIF format. This material is available free of charge via the Internet at http://pubs.acs.org.

JA907426S

(24) Altomare, A.; Cascarano, G.; Giacovazzo, C.; Guagliardi, A.; Burla, M. C.; Polidori, G.; Camalli, M. *J. Appl. Crystallogr.* **1994**, *27*, 435–436.
(25) Sheldrick, G. M. *SHELX97 - Programs for Crystal Structure Analysis*, Release 97-2; 1998.
(26) Farrugia, L. J. *J. Appl. Crystallogr.* **1999**, *32*, 837–838.
(27) Perdew, J. P.; Burke, K.; Ernzerhof, M. *Phys. Rev. Lett.* **1996**, *77*, 3865–3868.
(28) (a) Hohenberg, P.; Kohn, W. *Phys. Rev.* **1964**, *136*, B864–B871. (b) Kohn, W.; Sham, L. J. *Phys. Rev.* **1965**, *140*, A1133–A1138.
(29) Kresse, G.; Furthmuller, J. *Phys. Rev. B* **1996**, *54*, 11169–11186.
(30) (a) Blochl, P. E. *Phys. Rev B* **1994**, *50*, 17953–17979. (b) Kresse, G.; Joubert, D. *Phys. Rev. B* **1999**, *59*, 1758–1775.